Surface structure of coherently strained ceria ultrathin films

Yezhou Shi,[1,2] Kevin H. Stone,[2] Zixuan Guan,[1] Matteo Monti,[1] Chuntian Cao,[1] Farid El Gabaly,[3] William C. Chueh,[1,2,4] and Michael F. Toney[2,*]

[1]*Department of Materials Science & Engineering, Stanford University, 496 Lomita Mall, Stanford, California 94305, USA*

[2]*SLAC National Accelerator Laboratory, 2575 Sand Hill Road, Menlo Park, California 94025, USA*

[3]*Sandia National Laboratories, 7011 East Avenue, Livermore, California 94550, USA*

[4]*Stanford Institute for Materials and Energy Sciences, SLAC National Accelerator Laboratory, 2575 Sand Hill Road, Menlo Park, California 94025, USA*

(Received 25 April 2016; revised manuscript received 30 July 2016; published 14 November 2016)

Cerium oxide, or ceria, is an important material for solid oxide fuel cells and water splitting devices. Although the ceria surface is active in catalytic and electrochemical reactions, how its catalytic properties are affected by the surface structure under operating conditions is far from understood. We investigate the structure of the coherently strained CeO_2 ultrathin films on yttria-stabilized zirconia (001) single crystals by specular synchrotron x-ray diffraction (XRD) under oxidizing conditions as a first step to study the surface structure *in situ*. An excellent agreement between the experiment data and the model is achieved by using a "stacks and islands" model that has a two-component roughness. One component is due to the tiny clusters of nanometer scale in lateral dimensions on each terrace, while the other component is due to slightly different CeO_2 thickness that span over hundreds of nanometers on neighboring terraces. We attribute the nonuniform thickness to step depairing during the thin film deposition that is supported by the surface morphology results on the microscopic level. Importantly, our model also shows that the polarity of the ceria surface is removed by a half monolayer surface coverage of oxygen. The successful resolution of the ceria surface structure using *in situ* specular synchrotron XRD paves the way to study the structural evolution of ceria as a fuel cell electrode under catalytically relevant temperatures and gas pressures.

DOI: 10.1103/PhysRevB.94.205420

I. INTRODUCTION

Cerium oxide (CeO_2), or ceria, is an important ionic oxide compound used in many applications of catalysis [1], such as intermediate-temperature solid oxide fuel cells (SOFCs) [2], water splitting using concentrated solar power [3,4], and active materials and support for water-gas shift reactions [5,6]. The catalytic activity of ceria stems from two important aspects: (1) the redox reactions between the two oxidation states of cerium (Ce^{3+} vs Ce^{4+}) accompanied by the formation of oxygen vacancies and (2) the uncommon ability of ceria to retain the cubic crystal structure even when ~15% of the lattice oxygen anions are missing [7,8]. It was shown that the concentration of the reduced cerium cations and oxygen vacancies could be even higher on ceria surfaces [9] than in the bulk. Our recent spectroscopic analysis leads to the speculation that the surface reaction could be the rate-limiting step of a hydrogen evolution reaction (HER) on the ceria surface [10]. To better understand how the surface participates in the various catalytic reactions and how the surface structure evolves as a function of operating conditions, it is important to determine the atomic structure of the ceria surface under realistic conditions. In this paper, we employ specular synchrotron x-ray diffraction (SXRD) to obtain the structure of ceria ultrathin films at elevated temperature and ambient pressures. Structural modeling shows that the surface roughness is twofold: tiny clusters of islands on the local scale and long-range nonuniform film thicknesses across neighboring terraces. Distinguishing these two components is an important first step to understanding the role of surface structure on activity because the local roughness is likely involved in the catalytic activities of the ceria surface, whereas the long-range roughness is not.

We choose an oxide heteroepitaxial system of ceria films deposited on yttria-stabilized zirconia (YSZ) substrates for two reasons. Practically, ceria and YSZ are the materials of choice for anodes and electrolytes, respectively, in real-world SOFCs [11,12]. From the fundamental perspective, the surface of uniform, quasi-two-dimensional epitaxial film with well-defined crystallographic orientation is an ideal model system to study reactions occurring on the oxide surfaces. Recently, we demonstrated that highly crystalline, extremely flat ceria films can be grown commensurately to the YSZ substrate, which shares the same cubic fluorite structure as CeO_2, by pulsed laser deposition [13]. We use such oxide heteroepitaxy to examine the structure of ceria by *in situ* structural characterization.

Theoretical [14–18] and experimental studies [19–22] show that there are differences in the activities of various low-index planes of ceria, which could impact their catalytic behaviors. Since the high catalytic activity of ceria has been connected to the abundance of (110) and (001) surfaces in nanostructured ceria [19,23–25], we focus on the (001) orientation of ceria.

When commensurately grown on the vicinal (001) surface of YSZ single crystals, the surface normal of the ceria film is defined as the (001) direction. The fluorite structure has alternating planes of oxygens and cations along this out-of-plane direction. The (001) surface of ceria is the typical type III *polar* surface according to Tasker's definition for ionic crystals [26], where the surface is charged and a dipole moment exists in each bilayer of oxygen anions and cerium cations. Due to the dipole moment created in the out-of-plane direction perpendicular to the surface, the crystal

*mftoney@slac.stanford.edu

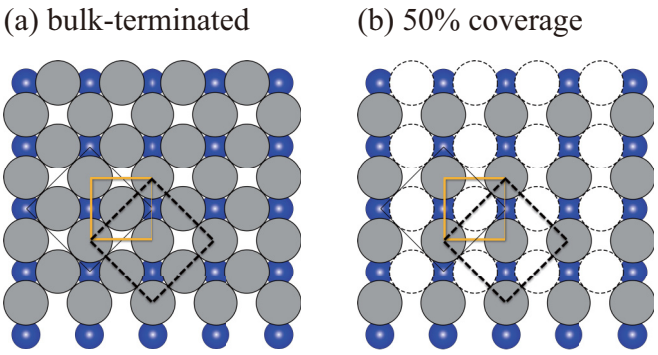

FIG. 1. Top view of the atomic arrangement of the first ML (oxygen anions, grey) and second ML (cerium cations, blue) of a CeO_2 (001) surface. The black square marks the conventional fluorite unit cell, whereas the yellow square marks the primitive unit cell on the surface. (a) Bulk terminated surface with 100% occupancy of oxygen on the topmost layer. (b) (1×1) relaxation with 50% occupancy of oxygen. This is one way of removing surface dipole consistent with a previous report [33]. The periodicity and size of the surface lattice remains unchanged, and there is no reconstruction.

is inherently unstable and expected to undergo significant changes to remove the polarity [27]. In general, there could be three mechanisms to achieve the polarity-neutral condition. First, adsorbates such as hydroxyl groups on the oxide surface may compensate for the excessive charge of the terminating surface layer [28,29]. The second is to induce surface *structural* reconstructions that remove a certain fraction of ions [30]. The last is through *electronic* reconstruction that redistributes the charges within the crystal so that the dipole is removed [31,32].

Despite considerable research performed on the ceria (001) surface, there is no consensus on the exact surface structure, which is probably dependent on the experiment environment. Earlier work used angle resolved mass spectroscopy [33,34] to show that the (001) surface was unreconstructed and terminated with a half monolayer (ML) of oxygen [Fig. 1(b)]. Later, Nörenberg and Harding [35] used a combination of scanning tunneling microscopy (STM) and low energy electron diffraction (LEED) to show that the single crystal ceria (001) surface could undergo subtle structural transformation under ultrahigh vacuum between several slightly different structures. More recent work has been performed on ceria epitaxial films and nanoparticles with the (001) facets for their technological relevance. It was shown that ceria (001) films of tens of nanometers exhibit a $c(2 \times 2)$ reconstruction after being annealed in an oxidizing atmosphere [36]. The LEED pattern was understood as having missing rows of oxygen atoms on the top surface. In another study, where ceria nanocrystals were grown on Ru (0001) substrates, both $c(2 \times 2)$ and (2×2) reconstructions were observed for the CeO_2 (001) facet, which were attributed to variations of the half coverage model or octopolar reconstruction (discussed in detail in Ref. [37]) that are consistent with polarity removal from a bulk terminated surface. In addition, there are other uncommon reconstructions or defect formation phenomena found on ceria nanoparticles that could be related to their finite size (e.g., the formation of Ce-O chain structure [38] or no relaxation at all [39]). Moreover, the discrepancies in the literature could arise from the different fabrication methods and the different substrate or support materials on which ceria was grown.

Note that many of the structural characterization techniques are electron based and require vacuum or ultrahigh vacuum conditions, making it challenging to extrapolate the solved structures into catalytically relevant conditions with an ambient or near-ambient atmosphere. Instead, we use a synchrotron-based technique, specular SXRD, to determine the surface and interface structure of ceria thin films [40,41]. A great benefit of hard x-rays is the large penetration depth and thus the ability to probe a crystal surface under gases and liquid conditions or even a buried solid-solid interface [42,43]. This characteristic makes SXRD an ideal tool for studying the surface structural changes *in situ* during catalytic reactions or thin film growth. The SXRD measures continuous intensity variation along the crystal truncation rods (CTRs), diffuse features in between the strongly scattering Bragg peaks [44,45] that arise from a flat, truncated surface of a single crystal or of an epitaxial film. The variation is extremely sensitive to the structural parameters of the surface or interface, including layer occupancies, atomic displacements, and the surface roughness.

In this paper, we used *in situ* SXRD to examine the surface and interface structure of the ceria-zirconia heteroepitaxy at elevated temperature under an oxidizing atmosphere. The CTR profile obtained from SXRD was refined using a stack averaging model that consists of three columnar stacks, each with a different film thickness. All the stacks are terminated with a half coverage oxygen ML that removes surface polarity and is consistent with our LEED measurement. Based on the good agreement between the simulation and the experiment data and our previous study on the thin film surface morphology, the roughness from the model fitting is interpreted as having two components. One component is due to the tiny clusters of atoms on each terrace that is otherwise flat. The other is the nonuniform ceria thickness on neighboring terraces, which could arise from a step depairing process during thin film deposition. The surface atomic structure of ceria thin films is resolved under ambient pressure. Our study paves the way to study the structural evolution of ceria surfaces under realistic temperatures (a few hundred degrees Celsius) and gas pressures of reducing atmosphere, where ceria is used as a fuel cell anode [2,46].

II. SAMPLE FABRICATION AND CHARACTERIZATION

The ceria ultrathin film was deposited on commercial YSZ substrates via pulsed laser deposition (PLD/MBE 2300, PVD Products). The ceria green target was pressed uniaxially from commercial CeO_2 powder (99.995%, Sigma Aldrich) and sintered at 1350 °C in 21% O_2 balanced Ar for 5 h. The one side polished, (001) oriented 9.5 mol % Y_2O_3 stabilized ZrO_2 single crystal substrates ($10 \times 10 \times 0.5$ mm) were supplied by CrysTec GmbH. The as-received substrates were sonicated in isopropanol for 15 min before being annealed in ultrahigh purity (UHP) Ar at 1250 °C for 12 h to produce atomically flat YSZ surfaces. Subsequently, ceria films were deposited in 0.5 mTorr UHP O_2 at ~500 °C. A KrF ($\lambda = 248$ nm) excimer laser was employed, and the laser spot was focused

to approximately 5 mm^2 on the target. The laser energy was calibrated as 80 mJ, and a repetition rate of 1 Hz was used. The substrate to target distance was kept at 100 mm. After the deposition, the samples were cooled down to room temperature in 0.5 mTorr background O_2. The film thickness was estimated, based on the number of laser pulses used, to be approximately 2.5 to 3.0 unit cells (UC). We have recently shown that CeO_2 films prepared under such conditions are coherently strained to the YSZ substrate up to 5 UC [13] despite the ∼5% lattice mismatch between the two materials. A reciprocal space map of a 1.8 nm (≈3.0 UC) thick film is shown in Fig. S2 in the Supplemental Material [49] and demonstrates coherence of the CeO_2 film in the range we consider here.

The LEED has been performed employing an Elmitec LEEM III, a commercial low-energy electron microscope. The adventitious carbon has been removed by annealing to above 350 °C in oxygen atmosphere, and sputtering procedures have been excluded to preserve the pristine surface. The diffraction pattern has been collected from a selected area of 8 μm diameter using a beam energy of 19 eV. The sample has been maintained a 500 °C in 10^{-6} Torr O_2 during the LEED experiment.

Topographical images of the YSZ and ceria surfaces were obtained using atomic force microscopy (AFM). We employed an XE-70 (Park Systems) instrument under the noncontact mode. Images of 2×2 μm were taken over multiple locations on the same sample. The line profiles on each image were extracted using the XEI software provided by Park Systems.

X-ray photoelectron spectroscopy (XPS) was used to determine the relative ratios of cations on the YSZ surface after high temperature annealing. A PHI spectrometer was employed with Al Kα radiation (x-ray energy of 1486 eV). The spectra were collected under ultrahigh vacuum ($<10^{-6}$ Pa) at room temperature at an exit angle of 20° with respect to sample surface. The XPS peaks near O2p, Y3d, and Zr3d regions were background subtracted and integrated using CasaXPS commercial software. The relative ratios of Y vs Zr were quantified by taking into account the atomic sensitivity factors of different species obtained from CasaXPS.

We performed specular SXRD at Beamline 7-2 at the Stanford Synchrotron Radiation Lightsource (SSRL), SLAC National Accelerator Laboratory. The sample was placed inside a custom-made *in situ* chamber, and specular rods were measured in a reflectivity geometry using a Pilatus 100 K two-dimensional (2D) pixel array detector [47,48]. We display specular diffraction data as a function of the scattering vector (which is perpendicular to the surface) in reciprocal lattice units (rlu) or normalized by the (001) peak position; this is defined as L. A fixed x-ray photon energy of 15.50 keV ($\lambda = 0.7999$ Å) was used. The x-ray beam size was defined as 0.5 mm (horizontal)× 0.6 mm (vertical) by slits to avoid beam spillover at small incident angles. The *in situ* SXRD was performed at 500 °C under the flowing gas of 1% O_2 balanced by N_2 with a total pressure of 1 atm. The oxidizing condition was intentionally chosen to ensure that all cerium species are oxidized and to avoid having Ce^{3+}, which could participate in the polarity removal on the (001) surface and change oxygen occupancies (as shown by STM under vacuum conditions [35]).

III. STRUCTURE DETERMINATION AND DISCUSSION

Before solving the interface and surface structures of the CeO_2-YSZ heterostructure, we obtained LEED on both a commensurate ultrathin film (∼3 UC) and a bulklike thick film (approximately 400 nm thick) as a control to verify the quality of the oxide surface. The LEED measurement was performed under a slightly oxidizing environment (10^{-6} Torr O_2) and at elevated temperature to compensate for the low electrical conductivity of undoped ceria. The bulklike film shows only (1×1) relaxation and no reconstruction. In contrast, we observe a weak $c(2 \times 2)$ reconstruction on the ultrathin CeO_2 (see Fig. S1 in the Supplemental Material [49]). One possible structure is proposed for the $c(2 \times 2)$ reconstruction, where the periodicity of the topmost layer is changed by the slight in-plane displacement of oxygen atoms. Both the (1×1) and the $c(2 \times 2)$ LEED patterns could be consistent with the physical picture of removing 50% of the topmost layer. Assuming the surface is O terminated under an oxidizing atmosphere, this means 50% O is absent to cancel the otherwise polar surface of the CeO_2 (001) film. Quantitative analysis of the in-plane symmetry of the reconstructed ultrathin film will require a separate study.

A. CTR model fitting

Next, we measure the specular rod of the ultrathin film at elevated temperature under oxidizing conditions of ambient pressure by SXRD. Surface structure factors were extracted by integrating the scattering features within a region of interest on the Pilatus area detector and being corrected for various geometric factors [50]. Error bars to the structure factors were based on counting statistics during the specular rod measurement. Our CTR data were modeled and fitted using the GenX program [51] developed for SXRD and XRR data refinement. To gauge the goodness of fit, the figure of merit (FOM) used in the refinement was defined as the average absolution difference between the logarithm of the measured data and of the simulated values [47]

$$\mathrm{FOM} = \frac{1}{N}\sum_{n} |\log_{10}(F_{n,\mathrm{obs}}) - \log_{10}(F_{n,\mathrm{sim}})|$$

where N is the number of data points (usually in the hundreds, far exceeding the number of fitting variables, typically 10 to 20 variables), $F_{n,\mathrm{obs}}$ is the nth structure factor extracted from measured data and $F_{n,\mathrm{sim}}$ the nth simulated structure factor based on the atomic model. For our CTR data, there are 612 data points and 8–10 fitting parameters. The logarithm is used to reduce the contribution of large F values near the bulk Bragg peaks that are not sensitive to the surface structure and usually several orders of magnitude higher than those near the valley (called the "anti-Bragg points," e.g., $L = 3.0$ in 00L between 002 and 004 peaks, which are more surface sensitive).

It is possible to determine the roughness of the original YSZ surface and of the deposited CeO_2 film from CTR modeling. Conventionally, the surface roughness for metals and semiconductors is often modeled with the classical β roughness model by Robinson [44]. However, we find the model is inadequate to describe the roughness in heteroepitaxial *oxide* with ultrathin

overlayers. Moreover, it is challenging to build interdiffusion at the substrate-film interface into the β roughness model. An alternative is to use layer occupancy model, where the occupancies of individual layers are treated as variables. A practical downside is that it is more challenging to impose the stoichiometry and the polarity-neutral condition in the layer occupancy model.

We adopt the stack averaging model proposed by Yang [52], which allows us to impose some structural constraints, while maintaining the flexibility of modeling incomplete layer occupancies as the interface and surface roughnesses. The entire structure is composed of a few columnar stacks of slightly different film thicknesses, and the structure factor is modeled as the coherent sum of the individual stacks. The approach has some distinct advantages: (a) Each stack consists of a semi-infinite substrate and a film with a certain thickness. The occupancies of the overall structure are controlled by varying the fractions of the stacks, rather than changing the occupancies of individual layers. (b) The vertical displacement of different stacks can be grouped together (more realistic picture than shifting atoms in a layer occupancy model). (c) Stoichiometry or a certain composition can be built into each stack, and the overall stoichiometry is maintained.

We start with the "stacks only" model, constructed as follows. First, we define a ML as one atomic layer of either cations or oxygens (in the fluorite structure, each unit cell consists of four MLs). The entire structure consists of three vertical stacks, or columns, with multiple MLs in each stack. Each stack has three components: the bulk YSZ substrate, the YSZ/ceria layer (close to the interface between YSZ and the CeO_2), and the CeO_2 overlayer. Within the starting model, the surface layer above the bulk consists of alternating layers of cations, and oxygen and is terminated with an oxygen layer, due to the oxidizing atmosphere and based on previous calculations [37]. Without the oxygen termination, no reasonable agreement between the data and fit can be reached. The thicknesses of the three stacks differ by one bilayer of ceria or, equivalently, one ML of oxygen anions and one ML of cerium cations. Since only the specular rod was measured, we treat each ML as a laterally uniform slab without imposing any constraint on the in-plane symmetry or periodicity. A schematic drawing of the stacks model is shown in Fig. 2. Here, the grey and blue stripes represent a ML of oxygen anions and Ce cations, respectively. Shown in darker grey are 6 MLs of interfacial YSZ/ceria that are placed above the bulk YSZ and below the ceria layers. These interfacial YSZ are included in the model to account for possible diffusion of Ce into the substrate and relaxation of certain YSZ layers below the interface. For each stack, an additional 6, 8, or 10 MLs of ceria (representing the film) are added above the surface YSZ. The number of ceria MLs are chosen based on the estimated thickness (2.0 to 2.5 UC) of the ceria film. In our notation, the ML closest to the bulk YSZ has the smallest number (i.e., ML1), whereas the ML on the very top has the largest number. The three stacks are terminated with ML16, ML14, and ML12, respectively, for stack 1, stack 2, and stack 3. To be consistent with the half coverage model, the terminating O layer is constrained as 50% coverage in all stacks.

Major fitting variables include the fractions of the stacks, as well as the interlayer spacing of the top few layers (details included in the Supplemental Material [49]). In the stack averaging model, fractions of stacks are varied to generate occupancies of individual layers in the entire structure. The MLs in each stack are fixed at 100%, except for the topmost oxygen layer. The interlayer spacings, or vertical displacements, near the surface and the interface are allowed to change as well. We find that the spacings near the interface have minimal effect on the shape of CTR profile, and, consequently, we fix them

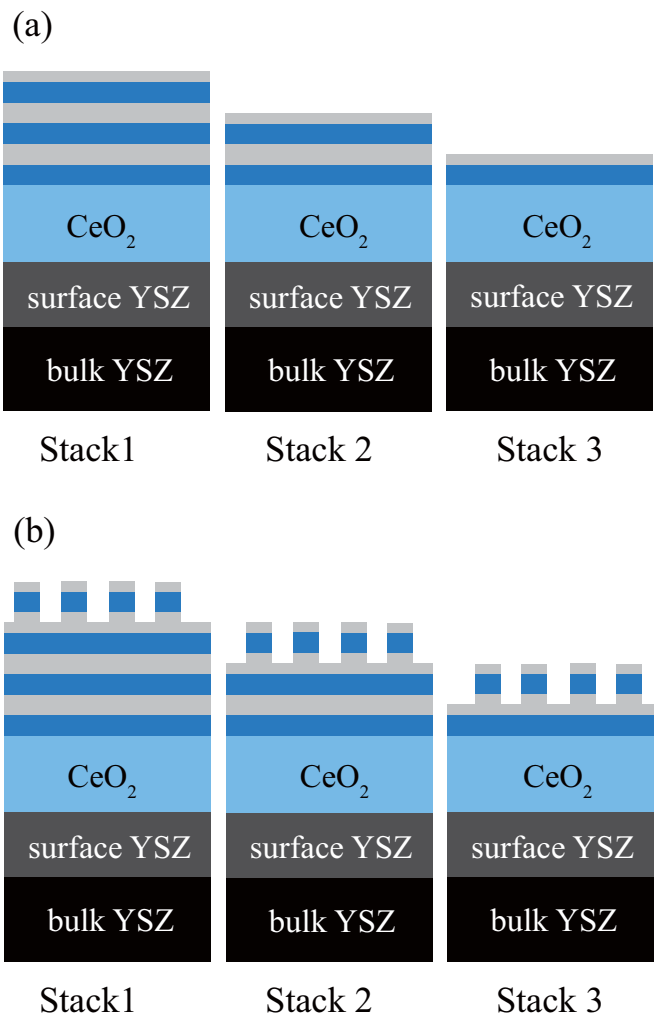

FIG. 2. Schematics of the two structural models in the CTR fitting. The grey and blue stripes near the surface represent the O^{2-} and Ce^{4+} MLs, respectively. (a) Stack only model: each stack consists of both the bulk YSZ, the interfacial YSZ and the ceria overlayer. The stack surface is oxygen terminated, with a fixed 50% oxygen occupancy. The thicknesses of neighboring stacks differ by one bilayer consisting of oxygen anions and cerium cations. (b) Stacks and islands model: an additional bilayer (of one Ce ML and one O ML) with low occupancies is introduced on top of each stack, representing islands on the thin film surface manifested as incomplete coverage. In both models, the fractions of each stack are variables. In the stacks and islands model, the occupancies of the island layer are also fitting parameters. In both models all layers of CeO_2, whether they represent layers or islands, and the YSZ substrate are coherent. The grey region labeled "surface YSZ" is a region where some intermixing of Ce and Zr(Y) is introduced into the CTR modeling.

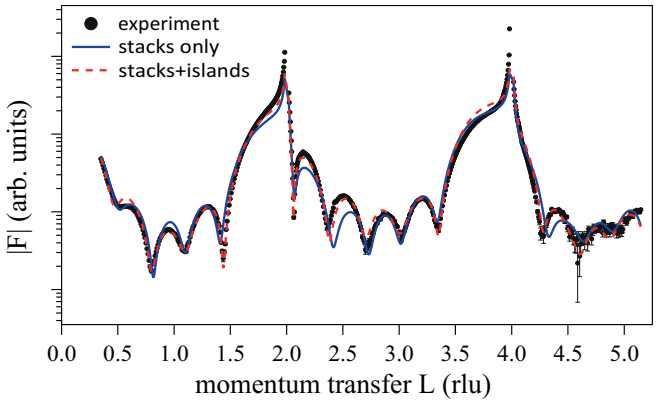

FIG. 3. Experimental data of the specular rod (00L) (blue circles) and the best of fits based on stack only model (solid blue curve) and the stacks and islands model (dashed red curve). The structure factors are plotted in log scale against the momentum transfer in the out-of-plane direction. The agreement is visually improved when the island layer are introduced on top of each terrace and the FoM is reduced.

at bulk values of YSZ and CeO_2 UC. For the CeO_2 film near the surface, the stacks are all the same except for their number of UC. The Debye-Waller factors of the atoms in the surface are not fitted because the CTR profile is rather insensitive to their exact values. Instead, they are fixed as 2.5 times their bulk values, which reflects the static and dynamic disorder at the surface. Similar values have been reported in the literature [53,54].

After refining the parameters, we obtain a reasonable agreement between the experiment (solid circles in Fig. 3) and the simulation (blue line in Fig. 3) in the stacks only model with a FoM of 0.102. In the first Ce layer above the ceria/YSZ interface (ML7 in Table SI, Supplemental Material [49]), the fitted occupancy is 92% rather than 100% of the atomic factor of Ce. The less than unity value is likely the result of diffusion of Zr cations into the ceria layer because Zr has a smaller atomic scattering factor. Since the number of electrons in Zr^{4+} is 36 and that in Ce^{4+} is 54, we estimate the fraction of Zr to be approximately 21% in the layer. The mixing of zirconium into the first layer of cerium may help to reduce the in-plane lattice constant of the first layer and therefore alleviate the large interfacial strain and help stabilize the deposited film. We also note that the occupancy of the first cation layer below the interface (ML5 in Table SI [49]) and that of the second cation layer above the interface (ML9 in Table SI [49]) are both fitted to be 100%. This means that the interdiffusion is limited to the first cation ML *above* the ceria/YSZ interface. An alternative explanation of the 92% cation occupancy is that the original YSZ surface has some roughness: the surface is covered by roughly 21% Zr before the ceria deposition. For the very surface in the model, the occupancy of the topmost oxygen layer is fixed at 50%, consistent with the (1×1) LEED pattern (see Supplemental Material [49]). Even if we allow the occupancies of the topmost O ML to vary as a fitting parameter, we obtain the best occupancy of 46 to 48%. The fitted result shows that our structural model is indeed consistent with the half coverage model needed to remove the surface polarity. There is also slight relaxation of the top three MLs of the ceria surface, and the fitted values are included in the Supplemental Material [49].

Previously, we studied the growth mechanism of ultrathin ceria on YSZ and showed that around 2 UC the CeO_2 film started to roughen with the formation of tiny islands (a few nanometers in lateral directions and less than 1 UC in the vertical direction) on the nominally flat terrace [13]. These tiny islands are demonstrated by the atomic force micrographs in Fig. S3 in the Supplemental Material [49], showing both the smooth YSZ surface and the small scale roughness/islands that develop on the 2.5–3 UC ceria film. We model these islands by including one additional bilayer of Ce cations and O anions on the original stack only model. The occupancies of Ce and O layers are constrained to be below 25% on each of the three stacks to emulate the low coverage of these tiny islands and no specific shape of the islands is assumed. The modified structure is called the "stacks and islands" model [Fig. 2(b)]. The occupancies and the displacements of the island layers are grouped for all stacks. In the newly added bilayer representing islands, only the occupancy of the island Ce layer is set as a variable. The occupancy of the island O layer is fixed as half that of the island Ce layer, whereas the occupancy of the original half covered oxygen layer is the sum of 50% plus the one half of the island Ce occupancy. This way, we ensure that each stack is by itself charge balanced *and* polarity neutral. Our refinement gives an occupancy of 23% Ce in the island and therefore 11.5% O in the island and 61.5% O in the third ML from the surface (originally the topmost O layer in the stacks only model). The displacements of the five MLs near the surface are allowed to change as well. Again, we obtain some moderate relaxations between 0.1 to 0.2 Å (refinement details can be found in Table SII in the Supplemental Material [49]).

Upon including the islands in the new model, the agreement is visibly improved (red line in Fig. 3). The FoM is also reduced to 0.065, a 35% reduction from 0.102 in the stacks only model. We point out that the results cannot be simply substituted by the β roughness model that defines an exponential decay of occupancies towards the surface [38] and was developed for simple metal surfaces. The stack averaging model is more flexible than β roughness in terms of simulating the individual layer occupancies (e.g., more parameters) and hence can capture the surface morphology better. In the meantime, the stack averaging model allows us to impose the constraint of 50% top layer coverage on each and every stack to ensure that polarity is removed from the each stack, as well as the entire structure.

B. Interpretation of the surface roughness

When combining the three columns, the stack averaging model points to a large surface roughness that spans seven layers (from ML18 to ML12; see Table SII in Supplemental Material [49]) or more than 1.5 UC. Superficially, this seems to disagree with our report that the ultrathin film surface was very flat at this thickness [13], as examined by atomic force microscopy. Each terrace was close to being atomically flat within the resolution of our AFM, and the surface was decorated with tiny clusters of atoms or islands that are no more than 0.5 UC tall and a few nanometers in lateral

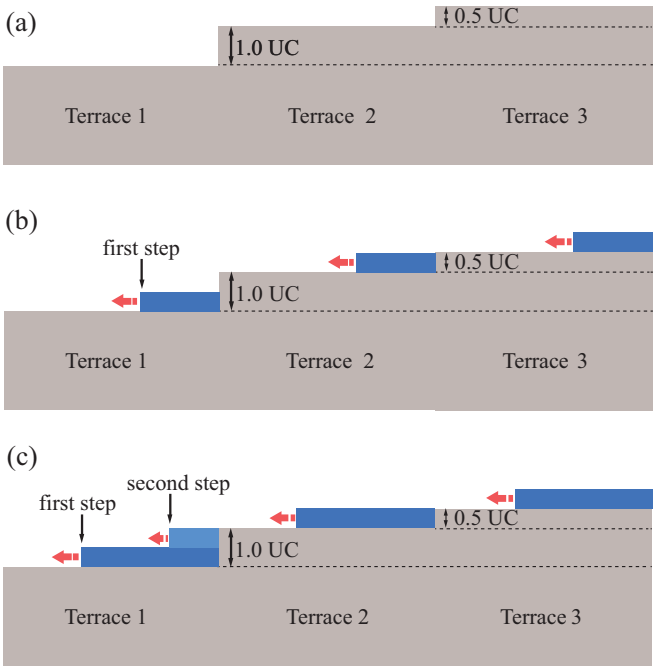

FIG. 4. Hypothesis of step depairing behind the observed nonuniform film coverage. (a) Step pairing occurs on the YSZ surface due to high-temperature annealing before deposition. The step height can be either 0.5 or 1.0 UC. (b) Due to the Schwoebel effect, the step of the film advances by incorporating adatoms primarily from the lower terrace (the terrace below the step on its left side). (c) As the first step advances on terrace 1, it leaves behind a second step between the film and the terrace to its right. The second step eventually advances as well by incorporating adatoms landed on the grown film. The original 1.0 UC step between the substrate terraces is broken into two 0.5 UC steps in the film. As a result, part of the CeO_2 film (to the right of the second step) grown on terrace 1 is one bilayer thicker than those grown on neighboring terrace 2 and 3.

dimensions. The tiny islands shown by AFM are consistent with the very low coverage of the topmost bilayer in the stacks and islands model, but they cannot explain the nonuniform coverage spanning *multiple* layers determined by CTR fitting. In other words, the large roughness is not simply decreasing layer occupancies from the bulk to the surface of the film, as sometimes observed for metal or semiconductor surfaces. We suggest this nonuniform film thicknesses over neighboring terraces arises from a step depairing process during the thin film growth. The idea is illustrated in Fig. 4.

When an atomically flat surface is created by high temperature annealing, ideally, the step height from one terrace to the next assumes the smallest possibly unit, and the terraces are uniform in their widths. In the case of a fluorite structure, the smallest step height is 0.5 UC or one bilayer of cerium ML and oxygen ML. In reality, step bunching or pairing can occur during annealing, giving rise to steps that are multiple times the smallest unit [55]. Indeed, we observed step bunching on YSZ surfaces after subjecting the as-received substrates to argon annealing.

When a substrate terrace is atomically flat and has complete coverage, there is no difference between the surfaces of neighboring terraces. This is true no matter whether the step height of one terrace to the next is bunched (paired) or not. All such substrate terraces would scatter x-rays identically, and their scattering amplitudes can be summed over the coherence length of x-rays [Fig. 4(a)]. If the deposited film has the same thickness across different terraces, the thin film would replicate the density and heights of the underlying substrate. When the surface interacts with x-rays, again, there is no difference between different terraces. Assuming uniform coverage (not necessarily complete) of neighboring terraces, the surface can be represented by a *single* stack made of YSZ substrate and an overlayer of a certain thickness and roughness, with no need to construct several stacks with slightly offset thicknesses.

The picture becomes very different if the deposited film has nonuniform coverage, that is, their thicknesses vary from one terrace to the next, or have different thicknesses on one substrate terrace. One terrace is no longer identical to the one next to it in terms of their scattering amplitude, and they cannot be represented by a single stack anymore. One possible way to generate nonuniform film thicknesses during thin film growth is via debunching of steps: the original large step (1.0 UC) on YSZ surface is separated, and the deposited film on the lower terrace of the original step has two terraces offset by the smallest step height of 0.5 UC.

The step debunching in the film is often related to the Ehrlich-Schwoebel (ES) effect [56,57]. The ES effect states that the energy barrier to adatom incorporation for adatoms diffusing from the upper terrace (above a step) is higher than the barrier for adatoms from lower terraces (below a step). In the extreme case, we can assume the step growth is dominated by the incorporation of adatoms from the lower terrace, while that from the upper terrace is inhibited. The growth rate of a step depends on not only the probability of adatom incorporation but also the terrace area, where larger terrace width leads to more adatoms under the same flux.

In an ideal case, where the terraces are separated by basic step heights of 0.5 UC, and there is equal spacing between steps, the steps would advance at the same rate (because of the uniform step width below different steps), and the film thickness should be uniform on different terraces. In reality, we already have bunched or paired steps on YSZ surfaces after high temperature annealing [cartoon illustrated in Fig. 4(a)]. When the ceria layer is deposited on the lower terrace of a 1.0 UC step, it leaves behind a 0.5 UC step. As the ceria layer continues to grow, the terrace (now a ceria layer) below the 0.5 UC becomes wide enough to accept adatoms as well [terrace 1 in Fig. 4(b)]. The adatoms on the first ceria layer could diffuse towards the 0.5 UC step and become attached, forming a second ceria layer. Since the substrate terrace below the first step is initially larger than the growing first layer (essentially the terrace below the second step), the advancement of the first step is faster than that of the second step. In other words, the original 1.0 UC step cannot advance together with the two ceria layers growing at the same rate. As a result, the original 1.0 UC step of YSZ substrate is debunched into *two* 0.5 UC steps in the film ([Fig. 4(c)].

To test the hypothesis depicted in Fig. 4**,** we performed atomic force microscopy on the *same* sample before and after the ceria deposition to compare the number of 0.5 and 1.0 UC steps. Each scan covered a square area of $2 \times 2\,\mu$m, and the measurement was repeated at more than 30 different

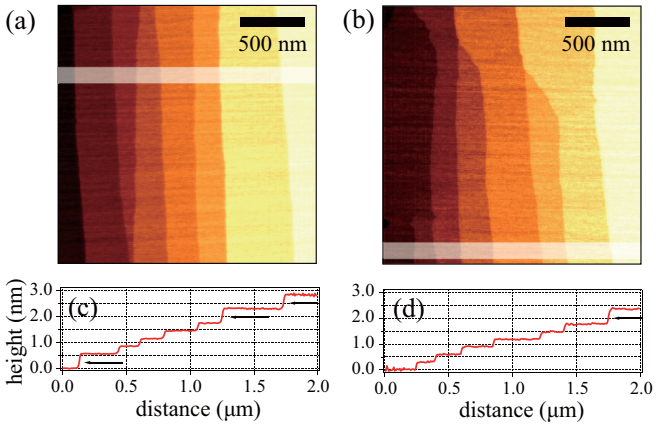

FIG. 5. AFM images (a) and (b) and line profiles (c) and (d) of the annealed YSZ (left column) and as-deposited CeO_2 surfaces (right column). The line profiles are averaged over the region included in the white window in the AFM images. The smallest, unpaired step in the fluorite structure is 0.5 UC (one bilayer of cerium cations and oxygen anions). Black arrows in the line profiles point at paired steps that are 1.0 UC tall where the rest of the steps are only 0.5 unit cells. Similar images were taken at more than 30 locations for both the bare substrate and the deposited film. Statistics of the steps can be found in Table I.

locations over a sample area of 5×5 mm. By counting the number of single steps (0.5 UC step height) and bunched steps (1.0 UC and occasionally 1.5 UC), we can calculate their relative fractions. Two examples are given in Fig. 5 for the substrate and for the film, respectively. Both the topographic images and the line profiles (averaged over the white stripe on the AFM image) of the step terraces are shown. The x axis of the line profile is the distance across the AFM image, and the y axis is the step height. The height of the leftmost terrace is arbitrarily set as zero. The 1.0 UC steps are indicated by arrows in the line profiles. The statistics collected over multiple locations are summarized in Table I. The fraction of 0.5 UC steps increase in ceria (71.3%) compared to the bare YSZ surface (64.0%) before deposition, whereas an opposite trend is observed for the 1.0 UC steps: the fraction goes down in ceria film (26.4%) than in the substrate (32.5%). The fraction of 1.5 UC step decreases as well, but statistically, the trend is less significant due to the limited number of 1.5 UC steps. The AFM results are consistent with the proposed process of step depairing that leads to the nonuniform ceria thicknesses across different terraces. The consistency justifies the use of multiple stacks of different film thicknesses, offset by 0.5 UC step heights, in the stack averaging models.

TABLE I. Statistics of the fractions of steps of different heights, measured at multiple locations on both the bare YSZ substrate and the deposited CeO_2 films. There is an increase of 0.5 UC steps on the ceria surface and a decrease of 1.0 UC steps. The result indicates that some of the 1.0 UC steps are depaired. We estimate the error bars in these fractions are a few percent, based counting statistics (>100 steps).

	0.5 UC steps (single)	1.0 UC steps (paired)	1.5 UC steps (paired)
YSZ (31 locations)	64.0%	32.5%	3.5%
CeO_2 (34 locations)	71.3%	26.4%	2.3%

Step bunching has also been reported for the strained overlayer [58,59] promoted by elastic interactions of steps. The fraction of 1.0 UC steps would increase if step pairing is favored. Although step bunching/pairing would increase the nonuniformity of film thickness as well, it is in conflict with our AFM observations. Therefore, step depairing due to the kinetic barrier is more likely to be operative in our system than further pairing.

The physical process we propose implies step flow growth rather than layer by layer (LBL) growth, at least at the beginning of the thin film deposition. Step flow may seem unlikely at a deposition temperature as low as ours at about 500 °C. We want to point out that the exact growth mode depends on an array of factors, including the deposition flux, the terrace width, and the kinetic barriers of adatom attachment from terraces to the steps. In principle, it is possible to estimate whether step flow or LBL is favored based on a few simple assumptions and the formalism developed by Hong *et al.* [60] for heteroepitaxial growth of oxide thin films. However, the surface diffusivity, an important parameter in the formalism, cannot be easily determined experimentally. Qualitatively, we know that the growth mode depends on the flux, as well as the terrace width at a given temperature [60]. Considering the relatively low flux of our deposition (~0.01 UC/s) and the moderate terrace width (typically 200 to 500 nm), step flow growth is possible in our case and cannot be simply ruled out on the basis of moderate deposition temperature.

IV. CONCLUSION

To summarize, we investigate the structure of the coherently strained CeO_2 ultrathin films on YSZ (001) single crystals using *in situ* surface x-ray diffraction under oxidizing conditions. The LEED shows that the surface has a weak $c(2 \times 2)$ reconstruction, consistent with a half coverage model, where 50% of the topmost oxygen anions is removed. We employ a stack averaging model that is composed of three columnar stacks to describe the large roughness of ceria, which spans over multiple MLs. The structural model is not only consistent with the surface from AFM but also with the polarity-neutral condition of the ceria on the macroscopic level, based on the surface symmetry revealed by our LEED measurement. A very good agreement between the experiment data and the model is achieved.

Importantly, our paper determines the surface structure of ceria under ambient pressures and at elevated temperature, which is a first step to study the surface evolution under catalytically relevant conditions. We show that the large roughness of the ceria surface is twofold: one is the short-range roughness due to nanometer-scale islands on each terrace and the other long-range due to nonuniform film thickness over different terraces. We attribute the nonuniform thickness to step debunching during the thin film deposition, a result of different incorporation rates of adatoms from the upper and the lower terraces of a step.

ACKNOWLEDGMENTS

This paper is financially supported by the Laboratory Directed Research and Development at the SLAC National Accelerator Laboratory DE-AC02-76SF00515. Portions of this research (SXRD) were carried out at the Stanford Synchrotron Radiation Lightsource (SSRL), a Directorate of SLAC National Accelerator Laboratory and an Office of Science User Facility operated for the U.S. Department of Energy Office of Science by Stanford University. Part of the work (AFM and XPS) was performed at the Stanford Nano Shared Facilities (SNSF). Sandia National Laboratories is a multiprogram laboratory managed and operated by Sandia Corporation, a wholly owned subsidiary of Lockheed Martin Corporation, for the U.S. Department of Energy National Nuclear Security Administration (Contract No. DE-AC04-94AL85000). We acknowledge the assistance from the staff at SSRL, especially A. Prado, B. Johnson, C. Troxel Jr., and R. Marks. Y.S. is grateful for insightful discussions with J. Stubbs, C. Schlepütz, H. Zhou, and D. Fong at the Advanced Photon Source, as well as helpful feedback on the manuscript from T. Petach at Stanford University.

[1] A. Trovarelli and P. Fornasiero, *Catalysis by Ceria and Related Materials* (Imperial College Press, London, England, 2002).
[2] A. Atkinson, S. Barnett, R. J. Gorte, J. Irvine, A. J. McEvoy, M. Mogensen, S. C. Singhal, and J. Vohs, Nat. Mater. **3**, 17 (2004).
[3] W. C. Chueh, C. Falter, M. Abbott, D. Scipio, P. Furler, S. M. Haile, and A. Steinfeld, Science **330**, 1797 (2010).
[4] Y. Hao, C.-K. Yang, and S. M. Haile, Chem. Mater. **26**, 6073 (2014).
[5] J. A. Rodriguez, S. Ma, P. Liu, J. Hrbek, J. Evans, and M. Perez, Science **318**, 1757 (2007).
[6] Q. Fu, H. Saltsburg, and M. Flytzani-Stephanopoulos, Science **301**, 935 (2003).
[7] M. Zinkevich, D. Djurovic, and F. Aldinger, Solid State Ionics **177**, 989 (2006).
[8] S. P. Ray, A. S. Nowick, and D. E. Cox, J. Solid State Chem. **15**, 344 (1975).
[9] W. C. Chueh, C. Falter, M. Abbott, D. Scipio, P. Furler, S. M. Haile, and A. Steinfeld, Chem. Mater. **24**, 1876 (2012).
[10] Z. A. Feng, F. El Gabaly, X. Ye, Z.-X. Shen, and W. C. Chueh, Nat. Commun. **5**, 4374 (2014).
[11] P. I. Cowin, C. T. Petit, R. Lan, J. T. Irvine, and S. Tao, Adv. Energy Mater. **1**, 314 (2011).
[12] D. J. Brett, A. Atkinson, N. P. Brandon, and S. J. Skinner, Chem. Soc. Rev. **37**, 1568 (2008).
[13] Y. Shi, S.-C. Lee, M. Monti, C. Wang, W. D. Nix, M. F. Toney, R. Sinclair, and W. C. Chueh, ACS Nano (2016), doi:10.1021/acsnano.6b04081.
[14] T. Sayle, S. Parker, and C. Catlow, Surf. Sci. **316**, 329 (1994).
[15] J. Conesa, Surf. Sci. **339**, 337 (1995).
[16] M. Baudin, M. Wojcik, and K. Hermansson, Surf. Sci. **468**, 51 (2000).
[17] Y. Jiang, J. B. Adams, and M. van Schilfgaarde, J. Chem. Phys. **123**, 064701 (2005).
[18] M. M. Branda, R. M. Ferullo, M. Causa, and F. Illas, J. Phys. Chem. C **115**, 3716 (2011).
[19] K. Zhou, X. Wang, X. Sun, Q. Peng, and Y. Li, J. Catal. **229**, 206 (2005).
[20] M. Tsuchiya, N. A. Bojarczuk, S. Guha, and S. Ramanathan, J. Chem. Phys. **130**, 174711 (2009).
[21] D. R. Mullins, P. M. Albrecht, T.-L. Chen, F. C. Calaza, M. D. Biegalski, H. M. Christen, and S. H. Overbury, J. Phys. Chem. C **116**, 19419 (2012).
[22] M. Tinoco, S. Fernandez-Garcia, M. Lopez-Haro, A. B. Hungría, X. Chen, G. Blanco, J. A. Perez-Omil, S. E. Collins, H. Okuno, and J. J. Calvino, ACS Catal. **5**, 3504 (2015).
[23] S. Carrettin, P. Concepción, A. Corma, J. M. Lopez Nieto, and V. F. Puntes, Angew. Chem., Int. Ed. **43**, 2538 (2004).
[24] W.-Q. Han, W. Wen, J. C. Hanson, X. Teng, N. Marinkovic, and J. A. Rodriguez, J. Phys. Chem. C **113**, 21949 (2009).
[25] H.-X. Mai, L.-D. Sun, Y.-W. Zhang, R. Si, W. Feng, H.-P. Zhang, H.-C. Liu, and C.-H. Yan, J. Phys. Chem. B **109**, 24380 (2005).
[26] P. Tasker, J. Phys. C **12**, 4977 (1979).
[27] C. Noguera, J. Phys.: Condens. Matter **12**, R367 (2000).
[28] G. E. Brown, V. E. Heinrich, W. H. Casey. D. L. Clark, C. Eggleston, A. Felmy, D. W. Goodman, M. Graetzel, G. Maciel, M. I. McCarthy, K. H. Nealson, D. A. Sverjensky, M. F. Toney, and J. M. Zachara, Chem. Rev. **99**, 77 (1999).
[29] L. K. Koopal, E. M. Lee, and M. R. Böhmer, J. Colloid Interface Sci. **170**, 85 (1995).
[30] C. Ebensperger and B. Meyer, Phys. Status Solidi B **248**, 2229 (2011).
[31] T. Higuchi and H. Y. Hwang, arXiv:1105.5779.
[32] G. Singh-Bhalla, C. Bell, J. Ravichandran, W. Siemons, Y. Hikita, S. Salahuddin, A. F. Hebard, H. Y. Hwang, and R. Ramesh, Nat. Phys. **7**, 80 (2011).
[33] G. S. Herman, Phys. Rev. B **59**, 14899 (1999).
[34] G. Herman, Surf. Sci. **437**, 207 (1999).
[35] H. Nörenberg and J. Harding, Surf. Sci. **477**, 17 (2001).
[36] V. F. Solovyov, T. Ozaki, A. Atrei, L. Wu, A. Al-Mahboob, J. T. Sadowski, X. Tong, D. Nykypanchuk, and Q. Li, Surf. Sci. **4**, 4627 (2014).
[37] Y. Pan, N. Nilius, C. Stiehler, H. J. Freund, J. Goniakowski, and C. Noguera, Adv. Mater. Interfaces **1**, 1400404 (2014).
[38] U. M. Bhatta, I. M. Ross, T. X. T. Sayle, D. C. Sayle, S. C. Parker, D. Reid, S. Seal, A. Kumar, and G. Mobus, ACS Nano **6**, 421 (2012).
[39] W. Lei, T. Zhang, L. Gu, P. Liu, J. A. Rodriguez, G. Liu, and M. Liu, ACS Catal. **5**, 4385 (2015).
[40] I. K. Robinson and D. J. Tweet, Rep. Prog. Phys. **55**, 599 (1992).
[41] R. Felici, in *Characterization of Materials*, edited by E. N. Kaufmann (John Wiley & Sons, Inc., Hoboken, NJ, 2012), Chap. 100, pp. 1–20.
[42] D. D. Fong and C. Thompson, Annu. Rev. Mater. Res. **36**, 431 (2006).
[43] D. D. Fong, C. A. Lucas, M. I. Richard, and M. F. Toney, MRS Bull. **35**, 504 (2010).
[44] I. K. Robinson, Phys. Rev. B **33**, 3830 (1986).
[45] A. Munkholm and S. Brennan, J. Appl. Crystallogr. **32**, 143 (1999).
[46] R. J. Gorte, S. Park, J. M. Vohs, and C. H. Wang, Adv. Mater. **12**, 1465 (2000).

[47] C. Schlepuetz, Ph.D. dissertation, University of Zurich, 2009.
[48] C. Schlepütz, R. Herger, P. Willmott, B. Patterson, O. Bunk, C. Brönnimann, B. Henrich, G. Hülsen, and E. Eikenberry, Acta Crystallogr. Sec. A **61**, 418 (2005).
[49] See Supplemental Material at http://link.aps.org/supplemental/10.1103/PhysRevB.94.205420 for LEED data, reciprocal space maps, atomic force microscopy, details of the X-ray diffraction, an explanation of the CTR fitting, and tables for the stacks only and stacks plus islands models.
[50] The CTR data correction procedures were done using Python Data Shell program (2014), (https://github.com/xraypy/tdl).
[51] M. Bjorck and G. Andersson, J. Appl. Crystallogr. **40**, 1174 (2007).
[52] Y. Yang, Ph.D. dissertation, University of Michigan, Ann Arbor, 2014.
[53] C. M. Schlepütz, M. Björck, E. Koller, S. A. Pauli, D. Martoccia, Ø. Fischer, and P. R. Willmott, Phys. Rev. B **81**, 174520 (2010).
[54] T. P. Trainor, P. J. Eng, G. E. Brown, I. K. Robinson, and M. De Santis, Surf. Sci. **496**, 238 (2002).
[55] A. Pimpinelli and J. Villain, *Physics of Crystal Growth* (Cambridge University Press, Cambridge, England, 1999), p. 88.
[56] G. Ehrlich and F. Hudda, J. Chem. Phys. **44**, 1039 (1966).
[57] R. L. Schwoebel and E. J. Shipsey, J. Appl. Phys. **37**, 3682 (1966).
[58] J. Tersoff, Y. H. Phang, Z. Zhang, and M. G. Lagally, Phys. Rev. Lett. **75**, 2730 (1995).
[59] F. Liu, J. Tersoff, and M. G. Lagally, Phys. Rev. Lett. **80**, 1268 (1998).
[60] W. Hong, H. N. Lee, M. Yoon, H. M. Christen, D. H. Lowndes, Z. Suo, and Z. Zhang, Phys. Rev. Lett. **95**, 095501 (2005).